A critical gradient model for energetic particle transport from Alfven eigenmodes: GYRO verification, DIII-D validation, and ITER projection

R.E. Waltz[1], E.M. Bass[2], and He Sheng[3]

[1]*General Atomics, P.O. Box 85608, San Diego, California, 92186-5608, USA*
[2]*University of California-San Diego, 9500 Gilman Dr., La Jolla, California 92093, USA*
[3]*Peking University, Beijing, China*

e-mail main author: waltz@fusion.gat.com

Abstract. Earlier work to develop a local critical gradient model (CGM) for stiff transport of energetic particles (EPs) from low-n Alfven eigenmodes (AEs) is reviewed and extended. The recipe for the critical EP density gradient based on the linear Alfven mode threshold is clarified and verified by recent GYRO code local nonlinear gyrokinetic simulations. The ALPHA code for the verified stiff AE critical gradient (as well as the weak passive high-n ITG/TEM) EP density transport is validated against a DIII-D discharge with significant NBI EP central core transport loss from AEs. The nonlocal EP drift orbit broadening of the locally determined critical gradient profile is important to the validation. An energy dependent CGM accounts for stronger AE transport of the higher energy EPs. Generalization of the ALPHA code and the CGM to include simultaneous AE drive from (and transport of) fusion alphas and 1 Mev NBI EPs is used in a revised in a projection of ITER EP central core losses. Interaction of the two EP species can double the individual transport losses when the total EP beta is doubled.

1. Introduction

Local nonlinear gyrokinetic code GYRO [1] simulations of energetic particle driven low-n Alfven eigenmodes embedded in high-n microturblence have motivated a local critical gradient model (CGM) for stiff energetic particle (EP) transport from Alfven eigenmodes (AEs). The critical gradient in the EP density gradient identified by the local linear low-n AE growth rate exceeding the ion temperature gradient and trapped electron mode (ITG/TEM) linear rate at the same low-n was first found in GYRO simulations of ITER fusion alpha driven AEs [2]. This recipe for the CGM has again been verified and made more precise by recent nonlinear GYRO simulations of a well studied neutral beam injected (NBI) DIII-D discharge (146102)[3] where about half the fast ions are lost from the inner half radius by AE induced transport. This CGM incorporated in the ALPHA EP density transport code, used in a previous ITER projection of AE fusion alpha loses [4], was validated by transported NBI pressure profile in good agreement with DIII-D experimental fast ion pressure profiles[5]. Simulations using a recently developed kinetic (energy dependent) radial EP transport code EPtran[6] illustrate the importance of EP drift orbit broadening of the critical gradient profile in the validation. A quasilinear theory based energy dependent CGM accounts for why higher energy EPs have stronger AE transport. Generalization of the ALPHA code and the CGM to include simultaneous AE drive from (and transport of) fusion alphas and 1 Mev NBI EPs in a revised projection of ITER EP losses is a key focus of the new work.

In Section 2, we clarify and verify the linear recipe for the CGM with nonlinear simulations. The ALPHA EP density transport code used to validate the CGM in Sec. 3, and project ITER CGM EP transport lost in Sec. 5, is formulated in Sec. 3. Section 6 summarizes our conclusions.

2. Alphen eigenmode linear rate recipe for the nonlinear critical density gradient

Local low-n Alfven eigenmodes are driven linearly unstable when the energetic particle *pressure* (or beta) gradient exceeds a critical value. Temperature gradient scales of the very hot particles are typically much weaker than their density gradient scales. Without significant approximation, it is more convenient to refer to a critical energetic particle *density* gradient. EP driven low-n AEs are not dissimilar in their effect to local ideal MHD or kinetic ballooning modes (KBMs). When the thermal plasma pressure (or beta) gradient exceeds an easily identified

critical value for linear stability, unbounded (infinitely stiff) transport follows and the local pressure gradient must relax quickly back to the linear critical gradient. Identifying the *nonlinear* critical gradient for unbounded AE transport of EPs from local low-n AE linear rate thresholds is more subtle because numerous AE mode branches as well as the ITG/TEM modes can be simultaneously unstable as the same low-n and with comparable growth rates. The AE modes are driven by both the EP gradients and the thermal plasma gradients.

Figure 1 from Ref. [2] illustrates a nonlinear GYRO [1] simulation of fusion alpha driven low-n AE modes embedded in high-n ITG/TEM turbulence for the GA-standard case with other ITER-like relevant parameters: $T_{EP}/T_e = 100$, $a/L_{nEP} = 4$, $a/L_{TEP} = 0$, and $0 < n_{EP}/n_e(\%) < 1.2$. The low-n AE modes like the TAE and EPM are unstable up to $k_\theta \rho_{EP} < 1$ (corresponding to $k_\theta \rho_s < 0.14$ and wave number $k_\theta = nq/r$) and the high-n ITG/TEM modes up to $k_\theta \rho_s \sim 1$. The most unstable AE mode (at $k_\theta \rho_s \sim 0.03$) becomes linearly unstable at $n_{EP}/n_e(\%) \sim 0.3$: $\gamma_{AE-ITG/TEM} > 0$. At that same wave number (same toroidal mode number n), the ITG/TEM mode branch unstable with $\gamma_{ITG/TEM} \sim 0.035[c_s/a]$ independent of $n_{EP}/n_e(\%)$. The peak high-n ITG growth rate is $0.21[c_s/a]$ at $k_\theta \rho_s \sim 0.3$. The EP particle diffusivity remains at low level ($D_{EP} \sim 0.8[(c_s/a)\rho_s^2]$) compared to the ion energy diffusivity ($\chi_i \sim 20[(c_s/a)\rho_s^2]$) until the AE branch growth rate starts exceed the (same low-n) ITG/TEM branch growth rate ($\gamma_{AE-ITG/TEM} > \gamma_{ITG/TEM}$) at $n_{EP}/n_e(\%) \sim 0.6$-0.7 where the AE transport is only slightly larger ($D_{EP} \sim 1.2[(c_s/a)\rho_s^2]$). At somewhat larger levels ($n_{EP}/n_e(\%) \sim 0.7-0.8$) so saturated state exist. The transport is unbounded and the EP density gradient must relax to the *nonlinear* critical gradient: $-dn_{EP}/dr|_{crit} \sim 0.008 \times 4[n_e/a]$. Note however that in such local nonlinear gyrokinetic simulations at fixed gradients, there is considerable uncertainty as to when the low-level transport is truly "saturated". These extreme multi-scale non-linear simulations are very expensive, which is why we need a *linear recipe* for the *nonlinear* critical gradient. Ref. [2] identified the linear recipe by $\gamma_{AE-ITG/TEM} = \gamma_{ITG/TEM}$ corresponding to $-dn_{EP}/dr|_{crit} \sim 0.006 \times 4[n_e/a]$ which is easily a factor two or more beyond the AE marginal stability threshold $\gamma_{AE-ITG/TEM} > 0$.

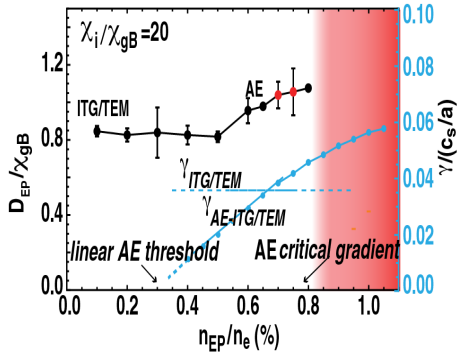

Fig. 1. Energetic particle diffusivity (black) and low-n ($k_\theta\rho_s$=0.14) mode growth rates (blue) versus fraction of fusion alpha particles for ITER-like GA-standard case parameters. [from Ref. 2].

To verify and clarify the linear recipe $\gamma_{AE-ITG/TEM} = \gamma_{ITG/TEM}$ on a physically realistic case, we recently made nonlinear local GYRO simulations for the well studied on-axis NBI DIII-D discharge 146102 known to have significant AE transport of the NBI EPs near a critical gradient [3]. DIII-D 146102 is a 1MA current, 2T magnetic field, and 4MW heated L-mode with a broad minimum safety factor profile: q=(5.2,4.5, 8.7) at r/a = (0., 0.5,and 1.0) respectively. (Other discharge details are given in Refs. [3,5].) Shot 146102 is in a series of DIII-D discharges demonstrating invariance of the fast ion profile to extreme variation in the NBI deposition profile found by mixing on axis deposition with increasing amounts of off-axis at constant total power. This is a clear experimental signature of stiff transport near a critical gradient.

A Maxwellian EP velocity space distribution was used in the GYRO simulations. Figure 2(a) shows the global AE growth rates spanning a broad maximum in toroidal mode number n from 2 to 6 and Fig. 2(b) shows the n=3 mode global electric field amplitude maximizing near r/a ~0.5 which is expected to be near the minimum in the local critical gradient. The low-n global modes take longer to form than local modes and are more likely to be broken up by the high-n ITG/TEM turbulence. Local mode stability should provide a better guide to the local critical gradient. Figure 3 illustrates the local nonlinear simulations at r/a=0.6 as the EP density profile is rescaled downward as a fraction or the classical slowing down (no transport) profile: $n_{SF} = n_{EP} / n_{SD}$. The scale factor identifying the *nonlinear critical gradient* is estimated to be $n_{SF} \sim 0.5$. Local nonlinear simulations at r/a=0.3 put the critical scale factor at $n_{SF} \sim 0.2$.

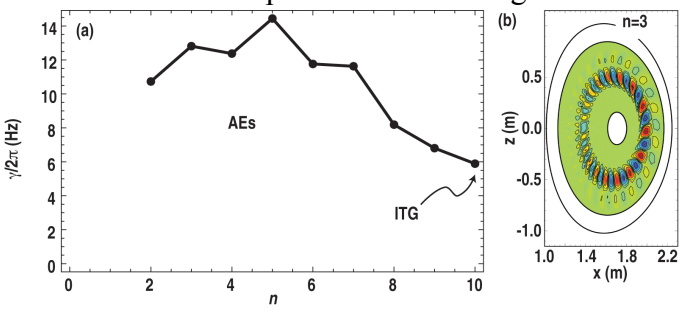

Fig. 2. Global Alfven eigenmode rates versus toroidal mode number n in (a) and electric field amplitude pattern for n=3 in (b) for DIII-D shot 146102.

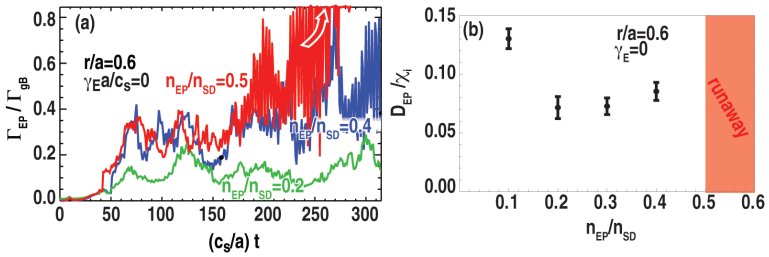

Fig. 3. GYRO simulated energetic particle flux versus time for increasing fraction of the slow-down density $\boldsymbol{n_{EP}/n_{SD}}$ at r/a=0.6 for DIII-D shot 146102 in (a). Energetic particle diffusivity normed to the thermal ion energy diffuivity versus $\boldsymbol{n_{EP}/n_{SD}}$ in (b).

Figure 4(a) [4(b)] show the n=3 linear growth rates at r/a=0.6 [0.3] versus the scale factor $n_{SF} = n_{EP} / n_{SD}$. $\gamma_{AE-ITG/TEM}$ (blue line) [γ_{AE} (red line)] refers AE rate with the thermal plasma gradients driving the n=3 ITG/TEM mode turned on [off]. The ITG/TEM rate $\gamma_{ITG/TEM}$ (green line) decreases slightly with increasing n_{SF} from the added Shafranov shift stabilization with added EP pressure. Note that in addition to the EP gradients, the thermal plasma gradients can drive the AE modes [e.g. Fig. 4(b)]. The linear recipe $\gamma_{AE-ITG/TEM} = \gamma_{ITG/TEM}$ verified by the nonlinear simulations $n_{SF} \sim 0.5$ [0.2] at r/a=0.6 [0.3] is encircled ("o"). As might be expected this is coincident with the linear threshold $\gamma_{AE} = 0$ (also encircled "o"). Unfortunately in many other cases, a straight line extrapolation to "zero" is not always so clear as it is here. It is better to construct our recipe from finitely growing rates. As $\gamma_{AE-ITG/TEM}$ "slips" below $\gamma_{ITG/TEM}$ the mode frequency shifts from a high frequency AE mode to the low frequency ITG (or TEM) mode. At the exact $\gamma_{AE-ITG/TEM} \equiv \gamma_{ITG/TEM}$ the AE and ITG/TEM modes co-exist with the same growth rate.

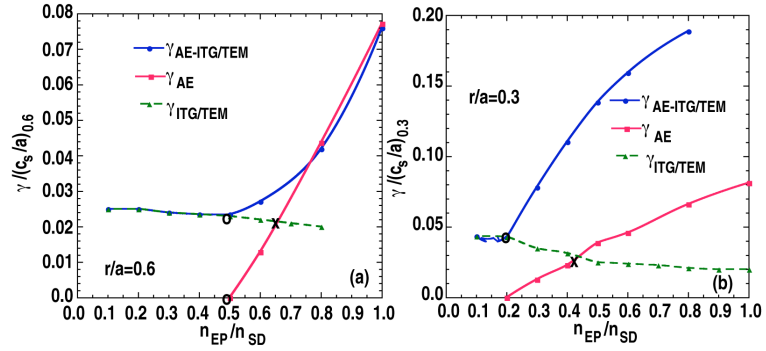

Fig. 4. GYRO (initial value) n=3 local mode rates versus fraction of the slowing-down density $\boldsymbol{n_{EP}/n_{SD}}$ at r/a=0.6 in (a) and r/a=0.3 in (b). "AE-ITG/TEM" ("AE") refers the the AEs with thermal gradient drives on (off). "ITG/TEM" has EP gradient drive off.

The exact point of transition (value of the critical n_{SF}) is not always so clear. The "crossing" $\gamma_{AE} = \gamma_{ITG/TEM}$ (identifies by "x") can be identified more accurately (particularly with initial value methods), however it is not as well verified. By linear simulations scanning n_{SF} at other radii, the critical gradient profile can be mapped out simply multiplying the slowing down EP density by n_{SF} as shown in Figure 5. The minimum critical gradient is little changed by the $\gamma_{AE-ITG/TEM} \equiv \gamma_{ITG/TEM}$ recipe is somewhat broader toward the center than the $\gamma_{AE} = \gamma_{ITG/TEM}$ recipe.

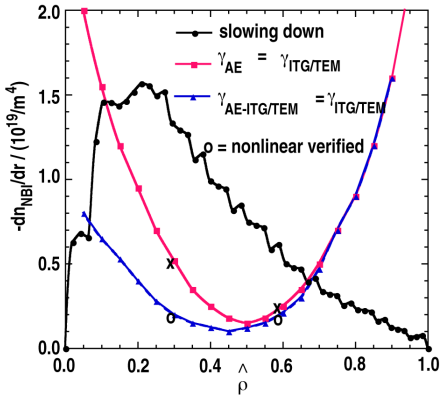

Fig. 5. Slowing-down EP gradient radial profile (black) and critical gradient profile using the $\gamma_{AE-ITG/TEM} = \gamma_{ITG/TEM}$ ($\gamma_{AE} = \gamma_{ITG/TEM}$) recipe in blue (red).

These high-q L-mode DIII-D discharge have relatively weak rotation and weak ExB shear: $\gamma_E / [c_s / a] = 0.023[0.010]$ at r/a=0.6[0.3]. ExB shear can increases the critical gradient. Modeling the critical gradient recipe by $\gamma_{AE-ITG/TEM} \equiv \gamma_{ITG/TEM} + \alpha_E \gamma_E$, the nonlinear simulations with artificially enlarged γ_E, found $\alpha_E = 2.2[0.39]$ to vary significantly. This is in contrast to the quench rule [7] for high-n ITG/TEM micro-turbulence $\gamma_{ITG/TEM}|_{\max} \sim \alpha_E \gamma_E$ where $\alpha_E \sim 1.0$ has weak parametric dependence. However for the weak shear rates at hand, the minimum critical gradient was increased by less than 20%.

3. Formulation of the ALPHA energetic particle density transport code and the CGM

For convenience, we repeat here the formulation of the ALPHA EP density transport code and the implementation of the CGM as first given in Ref. 4. The EP density continuity equation is

$$\partial n_{EP}(r) / \partial t - 1/V' \partial [V' D_{EP} \partial n_{EP}(r) / \partial r] / \partial r = S_0(r)[1 - n_{EP}(r)/n_s(r)] \quad [1]$$

where $S_0(r)$ is the source rate and $S_0(r)[n_{EP}(r)/n_S(r)]$ is the slowing down sink rate (to thermal plasma ions in the case of NBI or to Helium in the case of fusion alphas). $V' = d[2\pi^2 \kappa r R_0]/dr$ In the case of the DIII-D NBI simulations in Sec. 4, $S_0(r)$ is determined from the slowing down density $n_S(r)$ provide by TRANSP NUBEAM using the slowing down formula $S_0(r) = n_S(r)/\{\tau_S(r) I_2[a(r)]\}$ where τ_S is the slowing down time. From the standard Gaffey formulas [8] for the slowing down distribution, $I_n(\bar{a}) = \int_0^1 dx \; x^n / (\bar{a}^3 + x^3)$ where $\bar{a} = \sqrt{E_c / E_{EP}} = \sqrt{\hat{E}_c}$ is the square root ratio of the cross over energy and the EP birth (or injection) energy. $T_{EP} = (2I_4 / 3I_2) E_{EP}$ is the Maxwellian equivalent EP temperature. For ITER projections, the slowing down formula is used in reverse to get the slowing down density from the standard fusion alpha source rate. At the plasma edge (or pedestal top), the EP density boundary condition $n_{EP}(a)/n_S(a) = d_1$ assumes $0 < d_1 < 1$ with $d_1 = 0$ corresponding to orbit loss time much less than slowing down or transport times. ALPHA solves for the stationary state $\partial n_{EP}(r)/\partial t = 0$ integrating up the gradient with many iterations. Without transport $D_{EP} = 0 \Rightarrow n_{EP}(r) = n_S(r)$. The inner

core transport 'sink" has $n_{EP}(r) < n_S(r)$ with the outer core re-deposition "source" $n_{EP}(r) > n_S(r)$. A stiff EP driven AE transport is added to a weak ITG/TEM transport $D^{EP}_{ITG/TEM}$:

$$D_{EP} = D_{AE}(a/n_{EP})[(-\partial n_{EP}/\partial r) - (-\partial n_{EP}/\partial r)_{crit}]_{>0} + D^{EP}_{ITG/TEM} \quad [2]$$

where $(-\partial n_{EP}/\partial r)_{crit}$ is the critical gradient, and $[x]_{>0} = 0$ if $x < 0$. When $(-\partial n_{EP}/\partial r) > (-\partial n_{EP}/\partial r)_{crit}$, D_{AE} is taken to be arbitrarily large enough to drive the EP density gradient close enough to the critical gradient; larger values have no significant effect on the EP profile. The ITG/TEM transport is provide by the Angioni et al quasilinear ratio model [9,10]. $D^{EP}_{ITG/TEM}$ is normed to the effective thermal plasma energy diffusivity (see Refs. [3,4] for more details): $\chi_{eff} = E_{EP}\Gamma^{birth}_{EP}/[(-n_i\partial T_i/\partial r - n_e\partial T_e/\partial r)/2]$. The surface average transport flux is $\Gamma_{EP} = -D_{EP}\partial n_{EP}/\partial r$ and the flow is $V'\Gamma_{EP}$.

4. Validation against DIII-D discharges with energetic particle transport losses

Figure 6 (from Ref. [5]) illustrates the technique for validating the ALPHA EP density transport code and CGM by application to the DIII-D discharge 146102 series with on axis deposition (beam mix 0.0). The three component 80keV NBI beam was modeled by a single component injection energy of 64keV which gave a good fit to the NUBEAM-TRANSP EP effective temperature $T_{EP}(0.0,0.5,1.0 = (22,18,9.1)keV$ compared to the electron temperature $T_e(0.0,0.5,1.0 = (1.8,0.55,0.05)keV$. The electron density was $n_e(0.0,0.5,1.0) = (3.8,2.1,1.5)\times 10^{19} m^{-3}$. With the stiff AE transport "off" (green lines) there is a small reduction in the slowing down profiles (blue lines) from the ITG/TEM passive transport which cannot be discounted. As shown in Fig. 6(b) critical gradient profile for a beam-like slowing distribution (solid black lines) having more free energy is somewhat deeper and broader toward the center than the Maxwellian distribution (dashed black lines). The transported density gradient is pressed hard against the local critical gradient. (Ref. [5] was done before the verification in Sec. 2 and used the $\gamma_{AE} = \gamma_{ITG/TEM}$ recipe.) As shown in Fig. 6(d), about half the birth flow was transported from the inner mid radius (r/a~0.5) where it is re-deposited to the outer half radius. Only about 3% of the total birth flow is transported to the plasma edge.

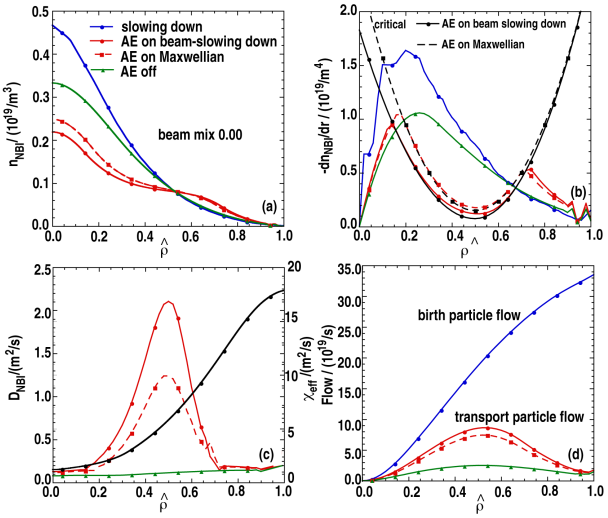

Fig. 6. ALPHA EP density transport code simulation of on-axis deposition DIII-D 146102. Radial profiles for the EP density in (a), density gradients in (b), effective particle diffusivity in (c), and flows in (d). (from Ref. [5]).

Figure 7 demonstrates the key experimental feature of stiff

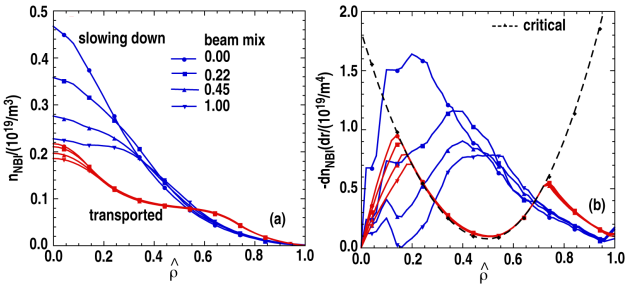

Fig.7. See caption Fig. 6 invariance of the transported EP profiles to increasing beam-mix of off-axis deposition (from Ref. [5]).

critical gradient EP transport. As the NBI deposition is shifted from on-axis to off axis (beam mix 0.0 to 1.0) at fixed input power, the slowing down EP density is less centrally peaked [Fig. 7(a)] and the mid-radius gradient is lower [Fig. 7(b)], but transported EP density profile remains largely unchanged.

Validation of the *local* EP critical *density* gradient model against the DIII-D experimental data clarified two points: the importance of *nonlocal* EP drift orbit broadening in DIII-D, and that higher energy EPs are transported more strongly by AEs. Figure 8 illustrates the validation using the NUBEAM-TRANSP kinetic EP transport code, which treats the 5D gyro-particle distribution function (with NBI deposition, slowing down, and pitch angle scattering). In principle the input diffusivity has a 5D dependence, but here the effective diffusivity from the ALPHA *density* transport code shown in Fig. 6(c) was input. The ALPHA $D_{EP}(r)$ in Eq. [2] refers to a flux surface average diffusion with no energy dependence. As shown in Fig. 8(a) about half the central core slowing down EP pressure was transported away in good agreement with the EFIT MHD experimental EP pressure. Perhaps more importantly, the NUBEAM-TRANSP predicted EP pressure profile shows no indication of the mid-core (r/a~0.5) flattening with sharp central peaking (r/a~ 0.0-0.2) shown in Fig. 7(a). Our interpretation is that the *local* EP CGM and the radially *local* (flux surface average) ALPHA density transport code does not allow for the 5D gyro-particle EP poloidal orbit drift off the flux surfaces. The EP's at the radial center outside the transport action region of the mid-core AE's where the *local* effective diffusivity is large, orbit drift into the region of large diffusivity. In effect the *local* critical gradient profile must broadened by a poloidal orbit half width as shown in Figure 9(a) from Ref. [6]. The DIII-D NBI EPs are mostly passing. The average orbit half-width was estimated to be $\Delta_{orbit}^{ave} = 1/2\langle v_{\|}\rangle_{ave}/\omega_{c\theta}$ where the ½ in indicates that a passing particle at the trapped-passing boundary has half the orbit half-width of a trapped particle. $\omega_{c\theta}$ is the poloidal ion cyclotron frequency and $\langle v_{\|}\rangle_{ave}$ is the EP distribution average velocity at the trapped-passing boundary. Fig. 9(b) illustrates the reduced central peaking using drift orbit broadening using the EPtran local kinetic transport code [6]. The orbit broadening in DIIID is large because of the high q_{min} ~ 4.5 needed to measure significant AE loss. It is perhaps overestimated here as the predicted pressure falls below the experiment.

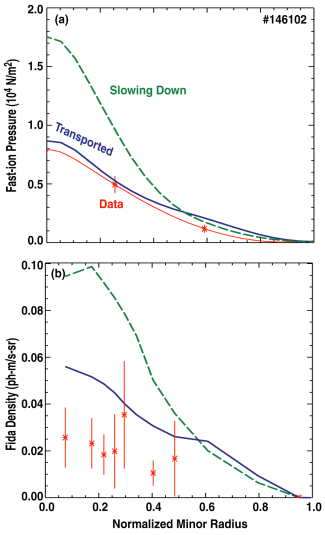

Fig. 8. The EP slowing down pressure (green dashed) and transported (blue) pressure from TRANSP-NUBEAM using the ALPHA effective EP diffusivity from Fig. 6(c), compared to the experimental EFIT EP pressure (red) profile in (a). The corresponding FIDA "density" profiles in (b). (From Ref. [5]).

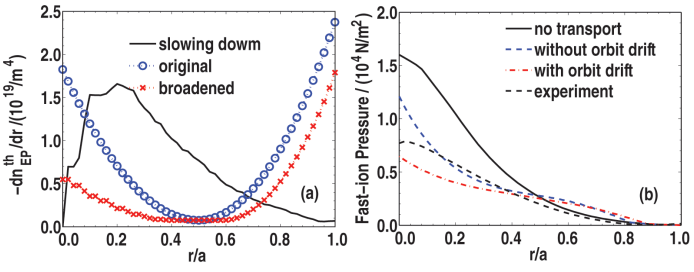

Fig. 9. Drift orbit broadening of the critical gradient profile used in Figs. 6 and 8 in (a) with the effect on the central peaking of the transported EP pressure profile in (b). (From Ref. [6]).

Figure 8(b) shows the NUBEAN-TRANSP slowing down compared to predicted FIDA "density" profiles corresponding to the Fig. 8(a) bulk pressure profiles. As expected from using an energy independent effective diffusivity, about half the FIDA EP "density", like half

the EP bulk pressure, is transported from the central core.

However the FIDA data suggests that at least three-fourths *appears* to be transported. This is explained by the fact FIDA "density" responds to EPs with energies higher that the bulk average energy: higher energy EPs are transported more strongly by AEs in accord with the quasilinear theory [4]. The simplest measure is the *coefficient of convection*: $C = Q_{EP}/[(3/2)T_{EP}\Gamma_{EP}]$ the ratio of energy flux to convective energy flux. Quasilinear GYRO gyrokinetic simulations in the AE threshold estimate C~1.7 [4]. This can be modeled with an energy dependent factor $G(\hat{\varepsilon}) = \Delta\hat{\varepsilon}^2/[(\hat{\varepsilon}-\hat{\varepsilon}_0)^2+\Delta\hat{\varepsilon}^2]$ inserted into the CGM effective AE diffusivity Eq. [2]. $\hat{\varepsilon} = E/T_{EP}$, $\hat{\varepsilon}_0$ represents AE energy resonances. $\hat{\varepsilon}_0$ and $\Delta\hat{\varepsilon}$ are fitted to C ~ 1.7 over an undistorted slowing down distribution. The resulting energy dependent CGM diffusivity $D_{EP}(r,E)$ is then treated in the *local kinetic* transport code EPtran [6] which can follow the AE transport distortions from the slowing down distribution. Again treating the DIII-D validation case (Fig. 6), it was found that resulting coefficient of convection was largely independent of the model for $G(\hat{\varepsilon})$ (i.e. could not be distinguished form $G(\hat{\varepsilon}) \equiv 1$). While variations in $G(\hat{\varepsilon})$ gave different transport distortions, C always approached the maximum corresponding to $Q_{EP} = E_{inj}\Gamma_{EP}$: $C_{\max} = E_{inj}/[3/2T_{EP}] \sim E_{inj}/[3/2T_{SD}] = 2.3$ for transport near the critical gradient. The interpretation is straightforward: for AE stiff critical gradient transport, the higher energy transported particles nearer the injection energy E_{inj} tend to be transported before they are slowed down [6]. In contrast the background high-n ITG/TEM turbulence which transports only the lowest energy EPs has C ~ 1/3 in DIII-D.

5. Projection of energetic particle transport losses in ITER

ITER will have two species of energetic particles: the fusion alpha particles and the 1 Mev NBI particles. The two EP specials separately and together drive AEs stable. Here we propose a simple recipe for generalization of the CGM to two EP species: the critical condition corresponds to $[-\partial p_\alpha/\partial r]/[-\partial p_\alpha/\partial r]_{crit} + [-\partial p_{NBI}/\partial r]/[-\partial p_{NBI}/\partial r]_{crit} > 1$ where $p_{EP} = T_{EP}n_{EP}$. In analogy to Eq. [2] both species have the same AE stiff CGM effective diffusivity but different ITG/TEM transport:

$$D_\alpha = D_{AE}(a/p_{tot})[(-\partial p_{eff}/\partial r) - (-\partial p_{eff}/\partial r)_{crit}]_{>0} + D^{\alpha}_{ITG/TEM} \quad [3a]$$

$$D_{NBI} = D_{AE}(a/p_{tot})[(-\partial p_{eff}/\partial r) - (-\partial p_{eff}/\partial r)_{crit}]_{>0} + D^{NBI}_{ITG/TEM} \quad [3b]$$

where

$$(-\partial p_{eff}/\partial r) = (-\partial p_\alpha/\partial r)\sqrt{(-\partial p_{NBI}/\partial r)_{crit}/(-\partial p_\alpha/\partial r)_{crit}} + (-\partial p_{NBI}/\partial r)\sqrt{(-\partial p_\alpha/\partial r)_{crit}/(-\partial p_{NBI}/\partial r)_{crit}}$$

and $(-\partial p_{eff}/\partial r)_{crit} = \sqrt{(-\partial p_\alpha/\partial r)_{crit}\cdot(-\partial p_{NBI}/\partial r)_{crit}}$. To illustrate the effect of the added 1 Mev NBI drive, the ITER fusion alpha projection of Ref. 4 is repeated. The $B_t = 5.3T$ and $I_p = 15MA$ *base case* thermal plasma profiles are projected by TGLF using the EPED1 projected H-mode pedestal beta $\beta_N = \beta_{ped}(\%)/[I_p/aB_t] = 0.92$ in Ref. 11. $Q = 10$ with $P_{aux} = 30MW$. $n_{ped} = 9\times10^{19}m^{-3}$ and $T_{ped} = 5keV$ with $n(0) = 10\times10^{19}m^{-3}$ and $T_i(0) = 15keV$. $\beta_{plas}(0) = 4.5\%$, $\beta_\alpha(0) = 0.5\%$, and $\beta_{NBI}(0) = 0.5\%$. Assuming the NBI critical density gradient of the 1 MeV NBI EP is 3.5 times higher than the 3.5 MeV fusion alphas, Figure 10 shows that doubling the total EP beta doubles the AE mid-core transport loses in both the fusion alpha and NBI channel over what would be expected with only self non-interactive AE drive. Note that 20% [30%] mid-core AE alpha [NBI] transport loss is recovered by re-deposition at outer radii with only 5%[10%] loss to EP birth flow by high-n ITG/TEM transport at the

edge. Since ITG/TEM transports only the lowest energy alphas (with very low C~ 1/30) escaping alphas amount to very hot Helium [4].

6. Discussion and Conclusion

The CGM linear growth rate recipe for AE stiff transport of EPs $\gamma_{AE-ITG/TEM} = \gamma_{ITG/TEM}$ first proposed in Ref. 10 has been recovered and verified in physically realistic GYRO nonlinear simulations of a DIII-D NBI discharge with significant AE loss from the central core. The recipe appears to be coincident with the linear AE threshold having the thermal plasma gradient drive discounted $\gamma_{AE} = 0$. Unfortunately, a simple recipe for the nonlinear ExB shear stabilization like $\gamma_{AE-ITG/TEM} = \gamma_{ITG/TEM} + \alpha_E \gamma_E$ with a constant α_E ~O(1), could not be verified. Unlike the DIII-D validation case, this poses a challenge for the discharges with significant ExB shear. Expensive nonlinear simulations may be required to identify the critical gradient profile (CGP). Significant broadening of the locally determined CGP by nonlocal orbit drift was required to explain the lack of strong central peaking in the high q_{min} DIII-D discharge. The CGM is consistent with higher energy EPs having the strongest AE transport: EPs at the injection energy are transported before they can slow down. Additional AE drive by the 1 Mev NBI in ITER can be expected to double the fusion alpha losses from the central core.

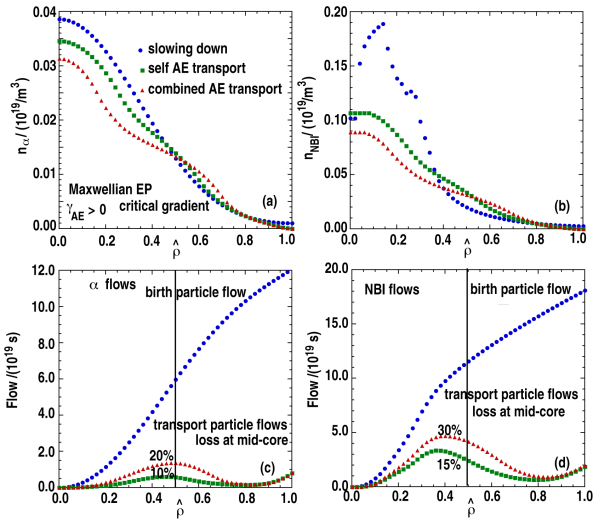

Fig.10. Fusion alpha [1 Mev] density and flow profiles in (a)[b] and (c)[d] for the ITER base case of Ref. [4]. Slowing down and birth flow in BLUE, self AE transport in GREEN , and combined AE transport in RED.

This material is based upon work supported by the U.S. Department of Energy, Office of Science, Office of Fusion Energy Sciences, Theory Program, under Award DE-FG02-95ER54309 and SciDAC-GSEP under DE-FC02-08ER54977. DIII-D data shown in this paper can be obtained in digital format by following the links at https://fusion.gat.com/global/D3D_DMP.

References

[1] J.M. CANDY and R.E. WALTZ, *Phys. Rev. Lett.* **91**, 045001 (2003) and *J. Comp. Phys.* **186**, 545 (2003).
[2] E. M. BASS E.M. and R.E. WALTZ, *Phys. Plasmas* **17**, 112319 (2010)
[3] W.W. HEIDBRINK, M.A. VAN ZEELAND, M.E. AUSTIN, E.M. BASS, K. GHANTOUS, N.N. GORELENKOV, B.A. GRIERSON, D.A. SPONG, AND B.J. TOBIAS,. *Nucl. Fusion* **53,** 093006 (2013)
[4] R.E. WALTZ and E. M. BASS, *Nucl. Fusion* **54**, 104006 (2014)
[5] R.E. WALTZ, E.M. BASS, W.W. HEIDBRINK, AND M.A. VANZEELAND, *Nucl. Fusion* **55**, 123002 (2015)
[6] HE SHENG and R.E. WALTZ, *Nucl. Fusion* **56** (2016) 056004
[7] R.E. Waltz, G.D. KERBEL, and J. MILOVICH, Phys. Plasmas 1, 2229, (1994)
[8] J.D. GAFFEY, JR., *J. Plasma Phys*.16 149 (1976)
[9] C. ANGIONI and A. PETERS, *Phys. Plasmas* **15**, 052307 (2008)
[10] C. ANGIONI et al., *Nucl. Fusion* **49**, 055013 (2009)
[11] J.E. KINSEY, G.M. STAEBLER, and R.E. WALTZ, *Nucl. Fusion* **51**, 083001 (2011)